PROCEEDINGS OF SCIENCE

Neutron Electric Dipole Moment from Beyond the Standard Model

Tanmoy Bhattacharya*
Los Alamos National Laboratory
E-mail: tanmoy@lanl.gov

Boram Yoon
Los Alamos National Laboratory
E-mail: boram@lanl.gov

Rajan Gupta
Los Alamos National Laboratory
E-mail: rajan@lanl.gov

Vincenzo Cirigliano
Los Alamos National Laboratory
E-mail: cirigliano@lanl.gov

We present an update on our calculations of the matrix elements of the CP violating quark and gluon chromo-EDM operators, as well as the operators these mix with, such as the QCD Theta-term. Their contribution to the neutron EDM is obtained by extrapolating the F_3 form factor of a vector current to zero momentum transfer. The calculation is being done using valence Wilson-clover quarks on HISQ background configurations generated by the MILC collaboration.

The 36th Annual International Symposium on Lattice Field Theory - LATTICE2018
22-28 July, 2018
Michigan State University, East Lansing, Michigan, USA.

*Speaker.

PoS(LATTICE2018)188

1. Introduction

Violation of the symmetry under simultaneous charge-conjugation and parity-flip (CP) is a core ingredient in the standard model (SM) and is necessary to explain the vast excess of matter over antimatter in the universe [1]. The SM CP-violation (CPV) is small and arises from the weak mixing between the quark [2, 3], and possibly also lepton [4, 5], families. Cosmological models require much stronger CPV [6], and most theories beyond the SM (BSM) do indeed produce it naturally. If this additional CPV is produced naturally by physics at a few TeV, the next generation of electric dipole moment (EDM) measurements [7, 8] are likely to find it, and the neutron is a very good candidate system. To connect theory to experiments, it is imperative to obtain the matrix elements (ME) of the CPV effective operators that control the EDMs of various particles. Here, we discuss our progress in calculating the neutron EDM (nEDM) due to the quark chromo-EDM operators.

1.1 BSM Operators

The SM CPV in the weak sector leads to effective dimension-6 four-fermion operators at hadronic scales. In principle, these also lead to dimension-3 CPV mass terms, $\bar{\psi}\gamma_5\tau\psi$, for the fermions, where ψ is the fermion field and τ is a flavor matrix.[1] Axial transformations can be used to remove the quark CPV masses, except when τ is the identity, in which case the anomaly transforms it to the dimension-4 gluon-topological-charge operator (also called the Θ-term), $G_{\mu\nu}\tilde{G}^{\mu\nu}$, where G is the gluon field strength [10]. Phenomenological estimates, using the limit on the neutron electric dipole moment, already constrain the total coefficient $\bar{\Theta}$ of this operator to be anomalously small, less than 3×10^{-10} [11].

In BSM theories, CPV operators start at dimension 6 at the weak scale [12], but two of them—the quark EDM (qEDM), $\bar{\psi}\tau\Sigma_{\mu\nu}\tilde{F}^{\mu\nu}\psi$, where F is the electromagnetic field tensor, and the quark chromo-EDM (qCEDM), $\bar{\psi}\tau\Sigma_{\mu\nu}\tilde{G}^{\mu\nu}\psi$—become dimension 5 after electroweak symmetry breaking. This means that their natural suppression relative to the QCD scale is by $v_{\text{EW}}/M^2_{\text{BSM}}$ rather than by $1/M^2_{\text{BSM}}$ as for the remaining dimension-6 operators—the gluon chromo-EDM (also called the Weinberg 3-gluon operator), $G_{\mu\nu}G_{\lambda\nu}\tilde{G}_{\mu\lambda}$, and various 4-fermion operators. In many BSM models, however, the dimension-5 operators come with extra Yukawa suppression, and their effect is comparable to the other dimension-6 operators. Thus, all these should be considered at the same level, and their ME within the neutron state calculated.

1.2 Form Factors

Using Lorentz symmetry, the response of a neutron to the vector current can be written in terms of the Dirac F_1, Pauli F_2, anapole F_A, and electric-dipole F_3 form-factors as

$$\langle N|V_\mu(q)|N\rangle = \overline{u}_N\left[\gamma_\mu\, F_1(q^2) + i\frac{[\gamma_\mu,\gamma_\nu]}{2}q_\nu\,\frac{F_2(q^2)}{2m_N} + (2i\,m_N\gamma_5 q_\mu - \gamma_\mu\gamma_5 q^2)\,\frac{F_A(q^2)}{m_N^2} + \frac{[\gamma_\mu,\gamma_\nu]}{2}q_\nu\gamma_5\,\frac{F_3(q^2)}{2m_N}\right]u_N\,,$$

[1] We ignore possible CP-violating Majorana phases in the neutrino sector [9]

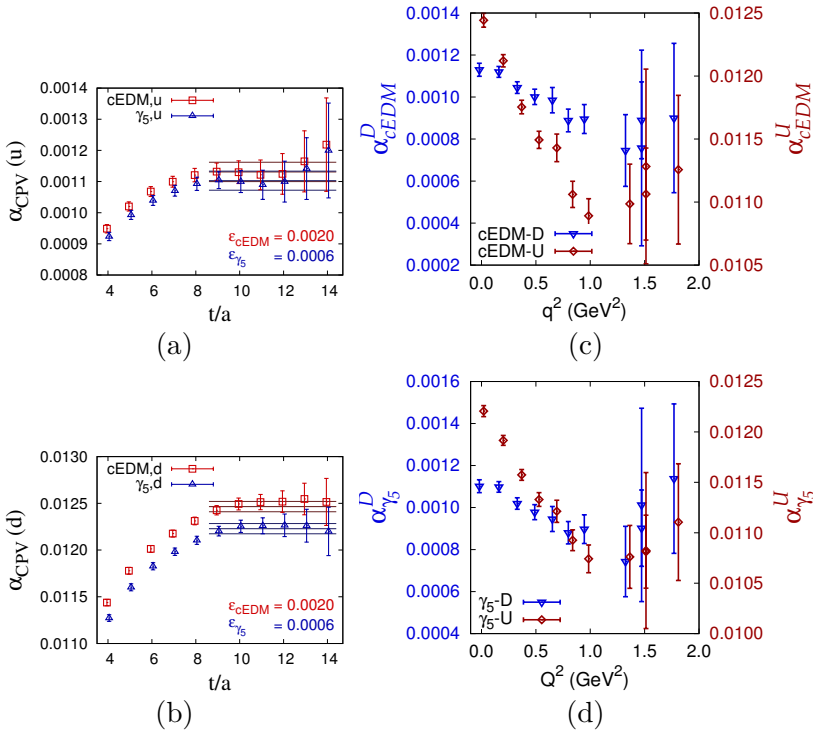

Figure 1: (a) The extraction of α_N with the insertion of the chromo-EDM (labeled cEDM) or CPV mass (labeled γ_5) operators on u quarks. (b) Same as (a), but with the insertion on the d quark. (c) α_N due to chromo-EDM insertion as a function of the 3-momentum of the neutron; the insertions on the u and d quarks are shown separately. (d) Same as (c), but for the CPV mass term.

in the Euclidean metric. Here V_μ represents the electromagnetic vector current, u_N represents the neutron spinor normalized such that $u_N\bar{u}_N = -i\not{p} + m_N$, where p is its momentum and m_N its mass, q the momentum inserted by the vector current V_μ, and $|N\rangle$ is the neutron state. The Sachs form factors [13–15] that describe the charge and current densities in the Breit frame, are related to these as $G_E \equiv F_1 - (q^2/4M^2)F_2$ and $G_M \equiv F_1 + F_2$.[2] The electric charge is $G_E(0) = F_1(0) = 0$ and the anomalous magnetic dipole moment is $G_M(0)/2M_N = F_2(0)/2M_N$. The anapole moment breaks the symmetry under simultaneous parity-flip and time-reversal (PT), and so, will be zero in our calculations. The electric dipole moment is given by the CP-violation form factor F_3 at zero q^2, $d_E = F_3(0)/2m_N$.

If parity is violated, an operator that creates an asymptotic neutron with the standard parity transformation properties is $N_{\alpha_N} \equiv \epsilon_{abc}\left[(\bar{d}^a)^C\gamma_5 P u^b\right]\exp\{i\alpha_N\gamma_5\}d^c$, where a, b, and c are color labels, the superscript C represents charge conjugation, $P \equiv (1+\gamma_4)/2$ is positive-energy projector for zero-momentum quarks that improves the signal,[3] and α_N is a constant depending on the asymptotic state that needs to be determined.[4] Under the standard choice of quark and neutron parities, α_N is real when PT is a good symmetry, imaginary when CP is good, and zero if parity is unbroken.

2. Status of Lattice Calculations and Preliminary Results

We have recently completed an analysis of the proton and neutron EDMs arising from the quark EDM [16]. Here we report on progress on nucleon EDMs arising from the quark

[2] In this frame, the form factor F_3 contributes a spin-dependent charge-density, and F_A, a current density.

[3] At nonzero momentum, this introduces a mixing with the spin-3/2 state, which being heavier than the neutron, is controlled like other excited states.

[4] α_N is also specific to the precise operator used: different operators with the same quark content and Lorentz properties can, in principle, need different α_N.

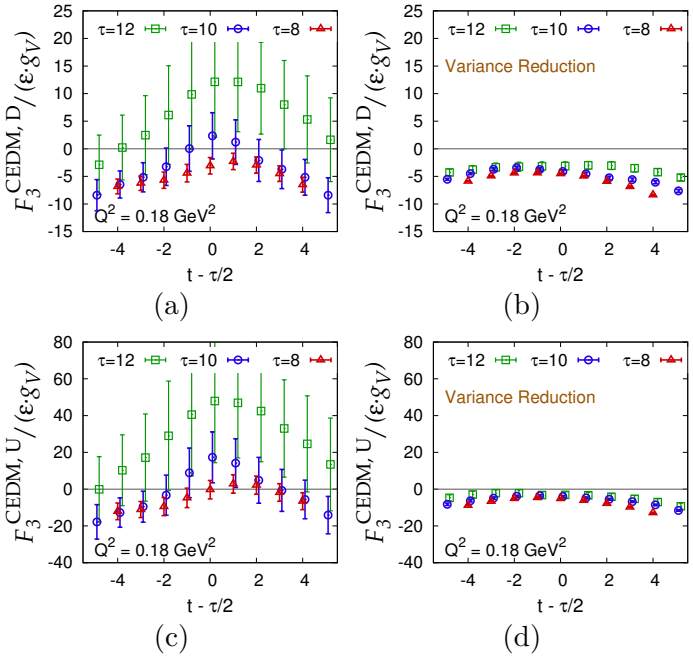

Figure 2: $F_3/(\varepsilon \cdot g_V)$ for the neutron due to chromo-EDM insertion on the d ((a) and (b)) and u ((c) and (d)) quarks before ((a) and (c)) and after ((b) and (d)) variance reduction. Here ε is the coefficient of the CP-violating term, and the baryonic vector charge g_V is unity in the continuum limit and cancels the lattice renormalization of the vector current.

chromo-EDM operator. This operator has power divergent mixing with lower dimensional pseudoscalar quark mass term and the gluon topological charge (if chiral symmetry is violated) that has to be controlled. We, therefore, discuss these operators as well.

The quark chromo-EDM operator is a quark bilinear, so its ME can be calculated using the Schwinger source method as described in previous proceedings [17, 18]. All the calculations presented here were done with Clover fermions on a MILC generated $L^3 \times T = 24^3 \times 64$ HISQ ensemble [19, 20] with lattice spacing $a = 0.1207(11)$ fm and pion mass $M_\pi^{\mathrm{sea}} = 305.3(4)$ MeV. The parameters of the Wilson-clover action used are $\kappa \approx 0.1272103$ corresponding to $M_\pi^{\mathrm{val}} = 310.2(2.8)$ MeV and $c_{\mathrm{SW}} = 1.05094$ determined using tree-level boosted perturbation theory with $u_P^{HYP} = 0.9358574(29)$. Statistical precision is increased using the truncated solver method [21, 22] with 128 low-precision and 4 high-precision measurements on each of the 1012 configuration. The quark-disconnected diagrams were ignored in all of the reported calculations.

To determine α_N, we use $\Im \mathrm{Tr}\gamma_5 \langle N_0 \bar{N}_0 \rangle / \Re \mathrm{Tr} \langle N_0 \bar{N}_0 \rangle$, where $\langle N_0 \bar{N}_0 \rangle$ is the propagator with $\alpha_N = 0$. Asymptotically, this gives $-2\tan\alpha_N$. Figures 1(a) and (b) show α_N extracted from the neutron propagator for the CP violation parameter ε in the small (linear) regime [17]. Figures 1(c) and (d) show that there is a strong dependence of the extracted α_N on the momentum of the neutron, probably due to lattice spacing artifacts.

The three point function, from which the ME of V_μ are extracted, calculated is

$$\langle \Omega | N_0(\vec{0},0) V_\mu(\vec{q},t) \overline{N_0}(\vec{p},T) | \Omega \rangle = \sum_{n,n'} e^{-i\alpha_n \gamma_5} u_n e^{-m_n t} \langle n | V_\mu(q) | n' \rangle e^{-E_{n'}(T-t)} \overline{u}_{n'} e^{-i\alpha^*_{n'}\gamma_5}$$

with projection onto only one spinor component using $\mathcal{P} \equiv \frac{1}{2}(1+\gamma_4)(1+i\gamma_5\gamma_3)$. The ME is isolated using the combination

$$R^\mu \equiv \frac{C^\mu_{3\mathrm{pt}}(q;\tau,t)}{C_{2\mathrm{pt}}(\tau;0)} \sqrt{\frac{C_{2\mathrm{pt}}(t;0) C_{2\mathrm{pt}}(\tau;0) C_{2\mathrm{pt}}(\tau-t;-q)}{C_{2\mathrm{pt}}(t;-q) C_{2\mathrm{pt}}(\tau;-q) C_{2\mathrm{pt}}(\tau-t;0)}}$$

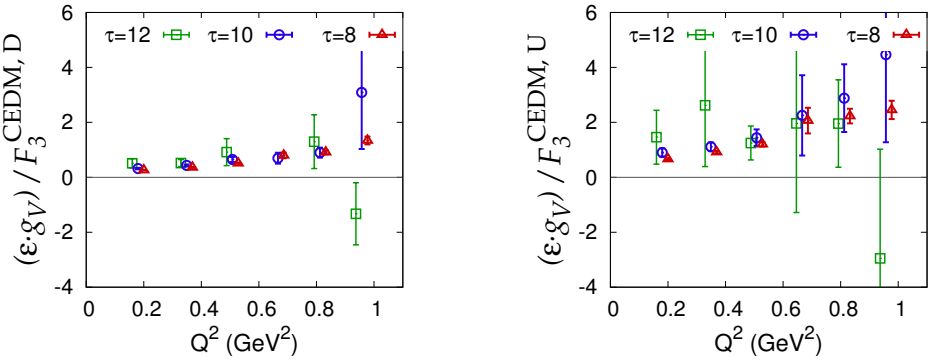

Figure 3: $(\varepsilon\cdot g_V)/F_3$ versus Q^2 for the neutron with chromo-EDM insertion on the d (left) and u (right) quarks at various source-sink separations.

where $C^{\mu}_{3\mathrm{pt}}$ are the projected 3pt functions and $C_{2\mathrm{pt}}$ are the real parts of projected 2pt functions. The eight quantities—$\Re R^{\mu}$ and $\Im R^{\mu}$—provide an overdetermined set from which the three form factors can be extracted.[5] In fact, these break up into two sets of four quantities: the components $V_R \equiv (\Re\vec{R}, i\Im R^4)$ give $G_2 \equiv G_E + \tan\alpha_N (Q^2/4m_N^2) F_3$, whereas the other four components $V_I \equiv (\Im\vec{R}, -i\Re R^4)$ give $G_1 \equiv G_M$ and $G_3 \equiv F_3 + \tan\alpha_N F_2$.[6] The overdetermined set of equations for the transition ME between a neutron at rest and momentum $(-\vec{q}, E_N)$ is

$$E \equiv \begin{pmatrix} X_1 & 0 & X_3 \\ 0 & Y_1 & 0 \end{pmatrix} \begin{pmatrix} G_1 \\ G_2 \\ G_3 \end{pmatrix} - \begin{pmatrix} V_R \\ V_I \end{pmatrix} = 0\,,$$

where $X_1 \equiv m(-cq_2, cq_1, s(E_N - m_N), -isq_3)^T$, $Y_1 \equiv m_N c(q_1, q_2, q_3, -i(E_N + m_N))^T$, $X_2 \equiv -(q_3/2m_N)Y_1$, $c \equiv \cos^2\alpha_N$ and $s \equiv \sin\alpha_N \cos\alpha_N$. We solve this set by the method of least squares, i.e., we solve the linear equations obtained by differentiating $E^T W E$ with respect to G_i for a positive weight matrix W, which we choose, for simplicity, to be $\mathrm{diag}(\sigma_R^2, \sigma_I^2)^{-1}$, where σ_R and σ_I are the errors on V_R and V_I respectively.

Figure 2 (a) and (c) show that the signal in the F_3^u and F_3^d is, a priori, poor. To improve the signal, we propose the following variance reduction method: use quantities z_i that are correlated with F_3 and have zero expectation value, and construct the lower variance estimator $F_3 - \sigma^2_{Fi}\Sigma^{-2}_{ij} z_j$, where Σ^{-2} is the inverse variance-covariance matrix of z_i and σ^2_{Fi} is the covariance of F_3 with z_i. Since we know that for $\varepsilon = 0$ (CP-symmetric case), F_3 is zero even at finite a and for our mixed action calculation, and remains highly correlated with F_3 for small ε, we expect using $F_3(\varepsilon = 0)$ as a z_i in the above expression will reduce the variance. Figures 2 (b) and (d) show that this variance reduction method improves the signal substantially.

[5] Note, we also consider R with momentum components permuted and reflected according to the symmetries of the theory, but do not display them explicitly in the narrative.

[6] One can also account for possible current nonconservation by including two additional form factors, a combination of which appears in each of the sets. The effects of including these neglected terms were found to be small. We also ignore purely lattice form factors (i.e., coefficients of hypercubic covariant, but not Lorentz covariant, tensors) including those arising from violation of the relativistic dispersion relation.

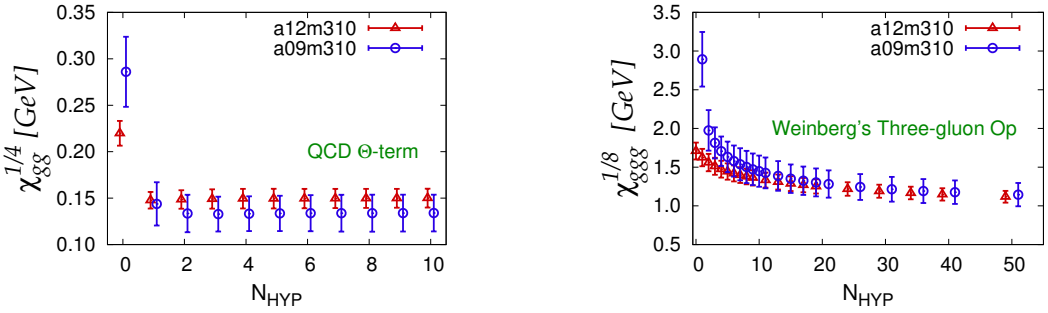

Figure 4: The evolution of the susceptibilities of the topological charge (left) and the Weinberg operator (right) as a function of the HYP smearing steps.

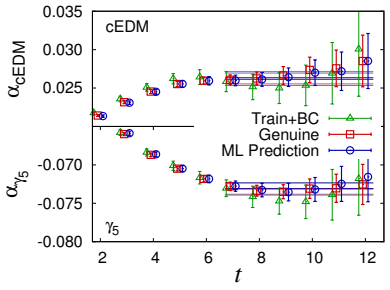

Figure 5: Comparison of the predicted and calculated imaginary part of the propagator with the insertion of the chromo-EDM and CPV mass term from the real part of the propagator with no insertion. Note that the final errors on the prediction are comparable to the actual errors, substantially reduced from the errors on the train set. These results are obtained using the choice of $\varepsilon_{\text{cEDM}} = 0.004$ and $\varepsilon_{\gamma_5} = -0.004$.

Figure 3 shows that $1/F_3$ behaves linearly with Q^2 as would be expected from pole-dominance. Also, the dependence on the source-sink separation τ is small, indicating excited state contributions are manageable. The next important step, once the signal is established, is to subtract power divergences in the renormalization due to operator mixing to ensure a finite result in the continuum limit.

3. Ongoing Work

We are extending the calculation of the chromo-EDM by constructing various combinations of the matrix elements that each provide an estimate of F_3, and by adding the contribution of the disconnected diagrams. To address divergent mixing under renormalization, the RI-sMOM scheme defined in [10] is complicated, so we are evaluating gradient-flow regularization [23]. We will first implement this scheme for the simpler case of the two gluonic operators. In Figure 4, we show the evolution of the susceptility of the scale-dependent Weinberg operator with the number of HYP smearings and compare it to the scale-independent topological susceptibility. We are investigating whether the expected scale-dependence persists under gradient-flow smearing. The motivation is that under gradient flow renormalization, the Weinberg operator needs no divergent subtraction. The next step will be to extend this to the fermion sector. To demonstrate efficacy, we will first compare results for isovector charges renormalized using the RI-sMOM scheme and gradient flow.

Finally, we are developing machine learning algorithms to reduce the computational effort. Building on the similarity to reweighting ensembles or unraveling quantum trajectories, the method proceeds by finding a combination of easily calculated and statistically precise quantities that have a high correlation with more compute-intensive quantities of interest, and then making the estimates rigorous by implementing standard bias reduction techniques. Initial tests of these ideas show promise as illustrated in Figure 5.

We acknowledge computer resources provided by LANL (IC), NERSC (US DOE contract DE-AC02-05CH11231), OLCF (US DOE contract DE-AC05-00OR22725) and JLAB (USQCD); the CHROMA software suite [24]; and support from US DOE contract DE-AC52-06NA25396 and LANL LDRD grant 20190041DR.

References

[1] Sakharov, A. D. *Soviet Physics Uspekhi* **34**(5), 392 (1991).

[2] Cabibbo, N. *Physical Review Letters* **10**, 531–533 (1963).

[3] Kobayashi, M. and Maskawa, T. *Progress of Theoretical Physics* **49**, 652–657 (1973).

[4] Pontecorvo, B. *Sov. Phys. JETP* **7**, 172–173 (1958). [Zh. Eksp. Teor. Fiz.34,247(1957)].

[5] Maki, Z., et al. *Progress of Theoretical Physics* **28**, 870–880 (1962).

[6] Trodden, M. *Rev. Mod. Phys.* **71**, 1463–1500 (1999).

[7] Semertzidis, Y. K. In *Journal of Physics Conference Series*, volume 335 of *Journal of Physics Conference Series*, 012012, (2011).

[8] Chupp, T., et al. arXiv:1710.02504 [physics.atom-ph] (2017).

[9] Xing, Z.-z. and Zhou, Y.-L. *Phys. Rev. D* **88**, 033002 (2013).

[10] Bhattacharya, T., et al. *Phys. Rev. D* **92**, 114026 (2015).

[11] Pospelov, M. and Ritz, A. *Nuclear Physics B* **573**(1), 177 – 200 (2000).

[12] Pospelov, M. and Ritz, A. *Annals of Physics* **318**(1), 119 – 169 (2005). Special Issue.

[13] Ernst, F. J., et al. *Phys. Rev.* **119**, 1105–1114 (1960).

[14] Barnes, K. *Physics Letters* **1**(5), 166 – 168 (1962).

[15] Hand, L. N., et al. *Rev. Mod. Phys.* **35**, 335 (1963).

[16] Gupta, R., et al. *Phys. Rev. D* **98**, 091501 (2018).

[17] Bhattacharya, T., et al. *PoS* **LATTICE2016**, 225 (2016).

[18] Yoon, Boram, et al. *EPJ Web Conf.* **175**, 01014 (2018).

[19] Follana, E., et al. *Phys. Rev. D* **75**, 054502 (2007).

[20] Bazavov, A., et al. *Phys. Rev. D* **87**, 054505 (2013).

[21] Bali, G. S., et al. *Computer Physics Communications* **181**(9), 1570 – 1583 (2010).

[22] Blum, T., et al. *Phys. Rev. D* **88**, 094503 (2013).

[23] Lüscher, M. *Journal of High Energy Physics* **2010**(8), 71 (2010).

[24] Edwards, R. G. and Joó, B. *Nuclear Physics B - Proceedings Supplements* **140**, 832 – 834 (2005). LATTICE 2004.